

Modeling the Black Hole Excision Problem

B. Szilágyi^{1,2}, H-O. Kreiss^{2,3}, and J. Winicour^{1,2}

¹*Department of Physics and Astronomy, University of Pittsburgh, Pittsburgh, Pennsylvania 15260*

²*Albert Einstein Institute, Max Planck Gesellschaft, Am Mühlenberg 1, D-14476 Golm, Germany*

³*NADA, Royal Institute of Technology, 10044 Stockholm, Sweden*

We analyze the excision strategy for simulating black holes. The problem is modeled by the propagation of quasi-linear waves in a 1-dimensional spatial region with timelike outer boundary, spacelike inner boundary and a horizon in between. Proofs of well-posed evolution and boundary algorithms for a second differential order treatment of the system are given for the separate pieces underlying the finite difference problem. These are implemented in a numerical code which gives accurate long term simulations of the quasi-linear excision problem. Excitation of long wavelength exponential modes, which are latent in the problem, are suppressed using conservation laws for the discretized system. The techniques are designed to apply directly to recent codes for the Einstein equations based upon the harmonic formulation.

PACS numbers: 04.25.Dm, 04.20.Ex, 04.30.Db, 95.30.Lz

I. INTRODUCTION

Two computational difficulties in simulating the emission of gravitational waves from black hole interactions are the existence of a singularities inside the black holes and a consistent treatment of the outer boundary so that the waveform of the gravitational radiation can be accurately extracted. Fortunately, the observable waves emanate only from the region outside the black holes and can be simulated, without loss of physical content, in a domain from which the singularities have been excised by introducing inner boundaries inside the black holes. However, the treatment of this domain by Cauchy evolution has had limited success. We present here a quasi-linear model excision problem whose mathematical analysis is simple enough to reveal some underlying computational pitfalls and the means to avoid them. In particular, we show that an accurate simulation of this model excision problem can be obtained by (i) blending together two evolution algorithms, one of which is well-posed near the outer boundary and the other well-posed near the inner boundary, where a superluminal evolution is employed, and (ii) incorporating discrete conservation laws which control spurious exponential growth. The results are aimed at numerical formulations of the Einstein equation as second order quasi-linear wave equations, such as in recent harmonic approaches [1, 2, 3].

The problem can be illustrated by considering the propagation of scalar waves on the fixed background geometry of a spherically symmetric Schwarzschild black hole. A choice of coordinates commonly adopted in numerical work for excising the singular region are ingoing Eddington-Finkelstein coordinates $x^\alpha = (t, r, \theta, \phi)$, in which the Schwarzschild spacetime metric $g_{\alpha\beta}$ is given by

$$g_{\alpha\beta}dx^\alpha dx^\beta = -\left(1 - \frac{2M}{r}\right)dt^2 + \frac{4M}{r}dtdr + \left(1 + \frac{2M}{r}\right)dr^2 + r^2(d\theta^2 + \sin^2\theta d\phi^2). \quad (1.1)$$

Here, the spacetime is foliated by the spacelike Cauchy hypersurfaces $t = \text{const}$, which are used to carry out the numerical evolution. The radial coordinate extends from the location of the singularity at $r = 0$ to the asymptotic region $r \rightarrow \infty$, to which the radiation propagates. The black hole is located at $r = 2M$. In the excision strategy, the simulation is carried out in a region $R_1 \leq r \leq R_2$, where the inner boundary satisfies $0 < R_1 < 2M$ and the outer boundary (introduced for the purpose of a finite coordinate range) satisfies $R_2 \gg 2M$.

The covariant wave equation for a scalar field u is

$$\frac{1}{\sqrt{-g}}\partial_\alpha(\sqrt{-g}g^{\alpha\beta}\partial_\beta u) = 0, \quad (1.2)$$

where $g = \det(g_{\alpha\beta})$ and $g^{\alpha\beta}$ is the inverse metric. In the above coordinates, it takes the explicit form

$$\begin{aligned} & -\left(1 + \frac{2M}{r}\right)\partial_t^2 u + \frac{4M}{r}\partial_t\partial_r u + \left(1 - \frac{2M}{r}\right)\partial_r^2 u + \frac{1}{r^2}(\partial_\theta^2 + \frac{1}{\sin^2\theta}\partial_\phi^2)u \\ & = -\frac{2M}{r^2}\partial_t u - \frac{2(r-M)}{r^2}\partial_r u - 2\cot\theta\partial_\theta u. \end{aligned} \quad (1.3)$$

Although this wave equation is non-singular and can be reduced to symmetric hyperbolic form in the region $R_1 \leq r \leq R_2$, it has some notable features which complicate a numerical treatment:

- The appearance of the mixed $\partial_t \partial_r$ derivative. This is an effect of the Eddington-Finkelstein coordinates in which the $(r, \theta, \phi) = \text{const}$ observers are moving relative to the time slicing. In the standard ADM [4] formalism, this gauge effect is described as a non-vanishing *shift*, described by the shift vector $\beta^\alpha = (0, \beta^r, 0, 0)$ where

$$\beta^r = \frac{1}{1 + \frac{r}{2M}} > 0. \quad (1.4)$$

- The change in sign of the coefficient of ∂_r^2 in passing across the black hole. This change in sign does not affect the hyperbolicity of the wave equation but it creates a horizon at $r = 2M$ across which waves cannot pass to the exterior. For $r > 2M$, the $(r, \theta, \phi) = \text{const}$ -observers move on timelike worldlines; for $r = 2M$, these worldlines are lightlike; and for $r < 2M$, they are spacelike. Thus, inside the horizon the ∂_t direction becomes spacelike, i.e. an evolution based upon grid points with constant r is superluminal inside the horizon.
- The energy density on the Cauchy hypersurface $t = \text{const}$ associated with a timelike vector ξ^α is $\mathcal{E} = \xi^\alpha T_{\alpha\beta} n^\beta$, where $n_\alpha = -(\partial_\alpha t) / \sqrt{-g^{\mu\nu}(\partial_\mu t)\partial_\nu t}$ is the unit timelike normal to the Cauchy hypersurface and

$$T_{\alpha\beta} = (\partial_\alpha u)\partial_\beta u - \frac{1}{2}g_{\alpha\beta}g^{\mu\nu}(\partial_\mu u)\partial_\nu u \quad (1.5)$$

is the energy momentum tensor of the scalar field u . In this paper we use the conserved energy associated with the choice $\xi^\alpha = t^\alpha$, defined by $t^\alpha \partial_\alpha = \partial_t$, whose flow leaves the Schwarzschild metric invariant. However, the corresponding energy density

$$\mathcal{E} = \frac{1}{2\sqrt{1 + \frac{2M}{r}}} \left(\left(1 + \frac{2M}{r}\right)(\partial_t u)^2 + \left(1 - \frac{2M}{r}\right)(\partial_r u)^2 + \frac{1}{r^2}(\partial_\theta u)^2 + \frac{1}{r^2 \sin^2 \theta}(\partial_\phi u)^2 \right) \quad (1.6)$$

is positive-definite and provides a norm for the scalar field only for $r > 2M$, where t^α is timelike. Inside the horizon, t^α is spacelike and \mathcal{E} represents momentum rather than energy density. This complicates the use of the energy method for establishing a stable algorithm in the interior of the horizon. The non-conserved energy associated with the choice $\xi^\alpha = n^\alpha$ does provide a global norm but we will not pursue that direction here. Instead, we use mode analysis to treat the inner region.

These features are further complicated by the consideration of proper boundary conditions for a numerical treatment. They are not peculiar to a second differential order treatment. In particular, all these features are prominent in a model excision problem based upon a first order symmetric hyperbolic treatment of the linear wave equation (1.3) carried out in Cartesian coordinates [5]. They are also prominent in another second order discussion of the excision problem [6], in which the energy norm associated with the choice $\xi^\alpha = n^\alpha$ is used to treat the stability of the evolution algorithm (2.8) which we adopt for the superluminal case.

We study the numerical simulation of the excision problem by introducing a model 1-dimensional system which retains all the geometric features of the full problem. In the domain $0 \leq x \leq 1$, we consider the quasi-linear wave equation

$$\begin{aligned} \partial_\alpha(\sqrt{-g}g^{\alpha\beta}\frac{1}{\Phi}\partial_\beta\Phi) &= \partial_t\left(\frac{\sqrt{-g}}{\Phi}g^{t\beta}\partial_\beta\Phi\right) + \partial_x\left(\frac{\sqrt{-g}}{\Phi}g^{x\beta}\partial_\beta\Phi\right) \\ &= -\partial_t\left(\frac{1}{\Phi}\partial_t\Phi\right) + \partial_t\left(\frac{a}{\Phi}\partial_x\Phi\right) + \partial_x\left(\frac{a}{\Phi}\partial_t\Phi\right) + \partial_x\left(\frac{b-a^2}{\Phi}\partial_x\Phi\right) \\ &= 0 \end{aligned} \quad (1.7)$$

where the coefficients are smooth and satisfy $b > 0$ and $a^2 > b$ for $x = 0$ and $a^2 < b$ for $x = 1$. These conditions ensure that the t -foliation is spacelike, that the metric determinant satisfies the Lorentzian requirement $g < 0$, that the outer boundary $x = 1$ is timelike and that the inner boundary $x = 0$ is spacelike. The shift vector has component $\beta^x = a$. We also require, analogous to (1.4), that $a > 0$ at $x = 0$, which ensures that the inner boundary is oriented so that all characteristics leave the domain. There is an event horizon at $a^2 = b$ across which waves cannot pass in the outer direction. For initial data satisfying $\Phi > 0$, the Cauchy problem for this equation is well-posed.

The non-linearity is introduced into (1.8) in order to model another computational difficulty related to the full Einstein equations. When harmonic coordinates are introduced to fix the gauge freedom, the Einstein equations reduce to quasi-linear equations for the components of the metric whose principle part is identical to (1.7). In these harmonic coordinates, there exists pure gauge solutions (flat metrics)

$$ds^2 = \Phi(-dt^2 + dx^2) + dy^2 + dz^2, \quad (1.9)$$

where

$$\Phi = 1 + f(t - x), \quad (1.10)$$

which describing traveling waves with profile $f > -1$. The simulation of (1.9) is one of the standardized tests proposed in the ‘‘Apples with Apples’’ project [7, 8], whose purpose is to compare different numerical treatments of the Einstein equations. The accuracy of the simulation is complicated by the existence of exponentially growing gauge waves [9]

$$ds_\lambda^2 = \Phi_\lambda(-dt^2 + dx^2) + dy^2 + dz^2, \quad (1.11)$$

where

$$\Phi_\lambda = e^{\lambda t}(1 + f(t - x)), \quad (1.12)$$

which solve the same equations and cannot be damped by dissipative techniques. For $\lambda \approx 0$, the Cauchy data for (1.11) approximate the Cauchy data for the test gauge wave (1.9). The excitation of this exponential error mode can dominate the simulation after a relatively short time. An accurate long term simulation of (1.9) requires controlling the excitation of (1.11) by some global method. Excellent long term accuracy has been obtained for the gauge wave test (with periodic boundaries) using a code [10] based upon a semi-discrete energy estimate derived at the linearized level by the *summation by parts* method [11, 12, 13]. Comparable results for the gauge wave test can also be obtained using analogs of the semi-discrete monopole conservation laws applied in Sec. IV to the quasi-linear wave equation (1.8). See [9] for details.

This quasi-linear wave equation closely models the gauge wave problem. Solutions of (1.8) can be used to construct gauge waves via (1.9). The traveling waves (1.10) and (1.12) are examples. Thus the accurate long term simulation of solutions to (1.8) can be complicated by the existence of neighboring solutions which grow exponentially in time, in precise analogy with the gauge wave problem.

We analyze the quasi-linear excision problem in terms of its elementary pieces. A stable algorithm for an initial-boundary value problem must also be stable for the corresponding linearized problem with frozen coefficients. This problem is considered in Sec. II. We consider three separate regions: (i) behavior of the interior evolution, (ii) behavior at a time-like boundary and (iii) behavior at a spacelike boundary. Treatment of a time-like boundary in general relativity introduces yet another computational difficulty related to the constraints. In the harmonic formulation of the initial-boundary value problem, each component of the metric satisfies a quasi-linear wave equation whose principle part is identical to (1.2). The only well-posed version of the initial boundary value problem which is known at present to preserve the harmonic constraints requires a Dirichlet boundary condition for some metric components and a Neumann boundary condition for the others [2]. For the purpose of future application of our results to harmonic evolution in numerical relativity, we concentrate here on such Dirichlet and Neumann boundary conditions, although the treatment extends to the general maximally dissipative boundary condition.

The spatial discretization of the wave equation in second differential order form has many advantages over first order formulations, as discussed in [14, 15]. These advantages have been recognized in recent second order harmonic approaches to numerical relativity [1, 2, 3]. For the case of zero shift, a comprehensive treatment of the wave equation in second order form has been given for both Dirichlet [16] and Neumann boundary conditions [17]. A major challenge of the excision problem is not just dealing with a shift but with a shift that is superluminal. This introduces complications even in the absence of boundaries. Standard implicit [18] and explicit [6] evolution algorithms for the second order wave equation with shift are unstable in the superluminal case. We treat this Cauchy problem in Sec. II A. In Sec. II B, we give a finite difference algorithm for the subluminal case which is stable for both Dirichlet and Neumann boundary conditions. We give a detailed analysis, since there is little treatment of the second order wave equation with shift in the literature. Whereas treatment of the Dirichlet condition carries over unchanged, a non-zero shift forces a revision in the treatment of the Neumann condition. The algorithm for the subluminal case (the outer algorithm) is well suited for treating the outer boundary of the excision problem but becomes unstable inside the horizon, where the shift is superluminal. In Sec. II C, we give an alternative finite difference algorithm (the horizon algorithm) which is stable in this region and admits a stable spacelike excision boundary.

We establish stability by using the method of lines to reduce the wave equation to ordinary differential equations in time on a spatial grid and then applying two standard techniques: mode analysis and semi-discrete energy estimates supplied by the summation by parts technique [20]. The energy method is important because it extends directly to the wave equation with non-constant coefficients in a region with inner and outer boundaries. We use the energy associated with the t -direction along which the spatial grid propagates. For the region inside the horizon, where this energy does not provide a positive-definite norm, we use mode analysis to establish a stable excision algorithm at the inner spacelike boundary.

In Sec. III we treat the linearized excision problem. This involves blending together the outer and horizon algorithms obtained in Sec. II. The additional ingredient is the necessity of non-constant coefficients in order to model a domain

with spacelike inner boundary and timelike outer boundary. The homogeneous Dirichlet and Neumann boundary conditions are constructed so that the energy of the semi-discrete system is conserved when the coefficients of the wave operator are time independent. In addition, the algorithm is constructed so that it conserves a monopole moment associated with the scalar field in the case of time-dependent coefficients.

The algorithm is implemented as a numerical code using a fourth order Runge-Kutta time integration. Two code tests of the linear excision problem are presented in Sec. III C: one where the data describe a pulse completely inside the horizon; the other where the data consist of an ingoing wave entering the outer boundary. The tests confirm the accuracy and stability of the finite difference algorithm.

In Sec. IV, we treat the excision problem for the quasi-linear wave equation. Although semi-discrete energy conservation is not considered in the nonlinear case, we construct the algorithm so that the scalar monopole moment remains conserved. Studies of the gauge wave problem [9] show that either energy conservation or monopole conservation are sufficient to suppress the exponential mode (1.12). This is confirmed in the numerical tests of the quasi-linear excision problem presented in Sec. IV B.

In Sec. V, we discuss the application to the harmonic Einstein equations of the algorithms developed here for the model excision problem.

II. ALGORITHMS FOR THE LINEAR WAVE EQUATION WITH CONSTANT COEFFICIENTS

We consider the wave equation

$$u_{tt} - 2au_{xt} - (b - a^2)u_{xx} = 0, \quad b > 0 \quad (2.1)$$

obtained from (1.8) by freezing the coefficients and making the linear approximation $\Phi \approx 1 + u$. (Where no confusion arises, we use the abbreviated notation $\partial_t u = u_t$, etc.) We treat three separate problems:

1. The interior Cauchy problem with both signs of $(b - a^2)$.
2. The initial-boundary value problem in the domain $0 \leq x < \infty$ with a timelike boundary at $x = 0$, i.e. $(b - a^2) > 0$.
3. The initial-boundary value problem in the domain $0 \leq x < \infty$ and a spacelike boundary at $x = 0$, i.e. $(b - a^2) < 0$.

If we can construct stable difference approximations for these three problems then the combined difference approximation for the full linear excision problem is also stable and the rate of growth is bounded independently of the step size. The reduction of the initial boundary value problem to Cauchy and halfplane problems is discussed in [19] and in Ch. 12 of [20].

A. The Cauchy problem

The Cauchy problem for (2.1) is well-posed for every fixed value of a and $b > 0$. The Fourier mode $u = \hat{u}e^{i\omega x}$ satisfies

$$\hat{u}_{tt} - 2ia\omega\hat{u}_t - (b - a^2)\omega^2 = 0, \quad (2.2)$$

with solution $\hat{u} = e^{\lambda t}$ where

$$\lambda = i\omega(a \pm \sqrt{b}). \quad (2.3)$$

Thus $\Re(\lambda) = 0$ and there are no exponentially growing modes

On a uniform spatial grid $x_\nu = \nu h$, consider the simplest second-order accurate finite difference approximation to (2.1),

$$W := u_{tt} - 2aD_0u_t - (b - a^2)D_+D_-u = 0, \quad (2.4)$$

where $D_0u_\nu = (u_{\nu+1} - u_{\nu-1})/(2h)$, $D_+u_\nu = (u_{\nu+1} - u_\nu)/h$ and $D_-u_\nu = (u_\nu - u_{\nu-1})/h$. The discrete Fourier mode $u_\nu = \hat{u}e^{i\nu\omega h}$ satisfies

$$\hat{u}_{tt} - \frac{2ia \sin(\omega h)}{h} \hat{u}_t + \frac{4(b - a^2) \sin^2(\omega h/2)}{h^2} \hat{u} = 0, \quad (2.5)$$

with solution $\hat{u} = e^{\lambda t}$ where

$$\lambda = \frac{ia \sin(\omega h)}{h} \pm \frac{i}{h} \sqrt{a^2 \sin^2(\omega h) + 4(b - a^2) \sin^2(\omega h/2)}. \quad (2.6)$$

For $b \geq a^2$ it follows that $\Re(\lambda) = 0$ but for $b < a^2$ there are exponentially growing modes, e.g.

$$\lambda = \pm \frac{2}{h} \sqrt{a^2 - b}. \quad (2.7)$$

for the shortest wavelength mode $\omega h = \pi$.

In order to remedy this problem, we consider the alternative second order accurate finite difference approximation

$$V := u_{tt} - 2aD_0u_t - (bD_+D_- - a^2D_0^2)u = 0 \quad (2.8)$$

for which the discrete Fourier mode satisfies

$$\hat{u}_{tt} - \frac{2ia \sin(\omega h)}{h} \hat{u}_t + \left(\frac{4b \sin^2(\omega h/2) - a^2 \sin^2(\omega h)}{h^2} \right) \hat{u} = 0, \quad (2.9)$$

with solution $\hat{u} = e^{\lambda t}$ where

$$\lambda = \frac{i}{h} \left(a \sin(\omega h) \pm 2\sqrt{b} \sin(\omega h/2) \right). \quad (2.10)$$

Now $\Re(\lambda) = 0$ for all values of the coefficients, subject to $b > 0$.

Unfortunately, because the evolution algorithm (2.8) involves a wider stencil than (2.4) it is difficult to analyze its behavior and design a clean algorithm near a timelike boundary. Accordingly, we will use the *outer algorithm* (2.4) near a timelike boundary and the *horizon algorithm* (2.8) in a region extending from the excision boundary to the exterior of the horizon.

B. Timelike boundary problem

We consider the initial-boundary value problem for (2.1) with $b - a^2 > 0$ in the domain $0 \leq x < \infty$. Without restriction we can assume $b - a^2 = 1$. Thus we consider the system

$$u_{tt} - 2au_{tx} - u_{xx} = 0. \quad (2.11)$$

We can derive an energy estimate. For real functions, let

$$(u, v) = \int_0^\infty uv \, dx, \quad \|u\|^2 = (u, u) \quad (2.12)$$

denote the L_2 -scalar product and norm. The energy of the system is

$$E = \frac{1}{2} \int_0^\infty (u_t^2 + u_x^2) dx = \frac{1}{2} (\|u_t\|^2 + \|u_x\|^2). \quad (2.13)$$

Integration by parts gives

$$\begin{aligned} \frac{1}{2} \partial_t \|u_t\|^2 &= (u_t, u_{xx}) + 2a(u_t, u_{tx}) \\ &= -\frac{1}{2} \partial_t \|u_x\|^2 - u_t(0, t)u_x(0, t) - au_t^2(0, t). \end{aligned} \quad (2.14)$$

We obtain energy conservation

$$E_t = \frac{1}{2} \partial_t (\|u_t\|^2 + \|u_x\|^2) = 0 \quad (2.15)$$

if the boundary condition at $x = 0$ is given by the Dirichlet condition

$$u_t(0, t) = 0 \quad (2.16)$$

or the Neumann condition

$$u_x(0, t) + au_t(0, t) = 0. \quad (2.17)$$

Note that the Neumann condition (2.17) involves the normal derivative $g^{x\alpha}\partial_\alpha = \partial_x + a\partial_t$ in the rest frame intrinsic to the boundary.

We now discuss the difference approximation

$$W_\nu := u_{\nu tt} - 2aD_0u_{\nu t} - D_+D_-u_\nu = 0, \quad \nu = 0, 1, 2, \dots \quad (2.18)$$

Corresponding to (2.12) we use the discrete scalar product

$$(w, v)_h = \frac{h}{2}w_0v_0 + \sum_{\nu=1}^{\infty} w_\nu v_\nu h. \quad (2.19)$$

Using Lemma 11.1.1 of [20], one can easily derive the summation by parts rules

$$(w, D_0v)_h = -(D_0w, v)_h - \frac{1}{4}(w_1 + w_{-1})v_0 - \frac{1}{4}(v_1 + v_{-1})w_0, \quad (2.20)$$

$$(w, D_-v)_h = -(D_+w, v)_h - \frac{1}{2}(w_1v_0 + w_0v_{-1}). \quad (2.21)$$

From (2.18),

$$\frac{1}{2}\partial_t \|u_t\|_h^2 = (u_t, u_{tt})_h = 2a(u_t, D_0u_t)_h + (u_t, D_-D_+u)_h. \quad (2.22)$$

Using (2.20) with w, v replaced by u_t , we obtain

$$2a(u_t, D_0u_t)_h = -\frac{a}{2}(u_{1t} + u_{-1t})u_{0t}. \quad (2.23)$$

Using (2.21) with w, v replaced by u_t and D_+u , respectively, we obtain

$$\begin{aligned} (u_t, D_-D_+u)_h &= -\frac{1}{2}\frac{\partial}{\partial t} \|D_+u\|_h^2 - \frac{1}{2}(u_{1t}D_+u_0 + u_{0t}D_-u_0) \\ &= -\frac{1}{2}\frac{\partial}{\partial t} \|D_+u\|_h^2 - \frac{h}{4}\frac{\partial}{\partial t} |D_+u_0|^2 - u_{0t}D_0u_0, \end{aligned} \quad (2.24)$$

i.e.

$$\frac{1}{2}\partial_t \left(\|u_t\|_h^2 + \|D_+u\|_h^2 + \frac{1}{2}|D_+u_0|^2 h \right) = - \left(D_0u_0 + \frac{a}{2}(u_{1t} + u_{-1t}) \right) u_{0t}. \quad (2.25)$$

Thus we obtain discrete energy conservation if we use the boundary condition

$$u_{0t} = 0 \quad (2.26)$$

or

$$\mathcal{N}_0 := D_0u_0 + \frac{a}{2}(u_{1t} + u_{-1t}) = 0, \quad (2.27)$$

corresponding to second order accurate approximations to the Dirichlet condition (2.16) or the Neumann condition (2.17).

The Neumann condition involves the *ghost point* $\nu = -1$, which we eliminate by means of (2.18) to obtain

$$-\frac{h}{2}W_0 + \mathcal{N}_0 = -\frac{h}{2}u_{t0} + D_+u_0 + au_{t1}. \quad (2.28)$$

We use (2.28) to update the boundary point via

$$u_{t0} - \frac{2}{h} \left(D_+u_0 + au_{t1} \right) = 0. \quad (2.29)$$

In the continuum problem, a homogeneous Neumann boundary condition also leads to conservation of the monopole quantity

$$Q = \int_0^\infty (u_t - au_x) dx. \quad (2.30)$$

This carries over to the conservation of the semi-discrete monopole quantity

$$Q = h \sum_{\nu=1}^{\infty} (u_{t\nu} - aD_0 u_\nu) + \frac{h}{2} (u_{t0} - aD_+ u_0), \quad (2.31)$$

i.e. $Q_t = 0$, when (2.29) is satisfied. This semi-discrete monopole conservation is extended to the non-linear problem in Sec. IV, where it has proved effective at suppressing the long wavelength slowly growing mode (1.12).

C. Spacelike boundary problem $0 \leq x < \infty$.

We now treat the initial-boundary value problem for (2.1) in the halfspace $0 \leq x < \infty$ for the case $a^2 > b$ with $a > 0$. The condition $a^2 > b$ implies that the boundary $x = 0$ is spacelike and the condition $a > 0$ implies that the boundary is oriented so that the characteristics leave the halfspace. Thus no boundary conditions are necessary in the continuum problem.

Since there is no energy estimate of type (2.15), we use mode analysis with frozen coefficients to formulate a stable discretization near the boundary. Consider first the continuum system. We study bounded solutions of the form

$$u = e^{st} \cdot \hat{u}(x), \quad \Re(s) > 0. \quad (2.32)$$

Introduction of this ansatz into (2.1) gives the ordinary differential equation

$$s^2 \hat{u} - 2as \hat{u}_x - (b - a^2) \hat{u}_{xx} = 0. \quad (2.33)$$

Thus u has the form

$$u = e^{st} (\sigma_1 e^{\mu_1 x} + \sigma_2 e^{\mu_2 x}) \quad (2.34)$$

where μ_j are the solutions of the characteristic equation

$$-s^2 + 2as\mu + (b - a^2)\mu^2 = 0, \quad (2.35)$$

i.e.

$$\mu_{1,2} = -\frac{as}{b - a^2} \pm \sqrt{\frac{a^2 s^2}{(b - a^2)^2} + \frac{s^2(b - a^2)}{(b - a^2)^2}} = \frac{as}{a^2 - b} \pm \frac{s\sqrt{b}}{a^2 - b}. \quad (2.36)$$

Since $a > \sqrt{b}$, all roots satisfy $\Re(\mu_{1,2}) > 0$ for $\Re(s) > 0$ and there are no bounded solutions. Thus the Kreiss condition (see [20], Ch. 10) is trivially satisfied and the problem is well posed.

As difference approximation for the halfplane problem we use the horizon evolution algorithm (2.8), i.e.

$$u_{\nu tt} - 2a \frac{(u_{\nu+1} - u_{\nu-1})_t}{2h} - b \frac{(u_{\nu+1} - 2u_\nu + u_{\nu-1})}{h^2} + a^2 \frac{(u_{\nu+2} - 2u_\nu + u_{\nu-2})}{4h^2} = 0 \quad (2.37)$$

for $\nu = 2, 3, \dots$. We need two extra boundary conditions to determine u_0 and u_1 . We use the extrapolation conditions

$$h^3 D_+^3 u_0 = 0, \quad h^3 D_+^3 u_1 = 0. \quad (2.38)$$

Now we study bounded solutions of type

$$u_\nu = e^{st} \sum_{j=1}^4 \sigma_j \kappa_j^\nu, \quad \Re(s) > 0 \quad (2.39)$$

where κ_j are solutions of the characteristic equation

$$\tilde{s}^2 - a\tilde{s}\left(\kappa - \frac{1}{\kappa}\right) - b\left(\kappa - 2 + \frac{1}{\kappa}\right) + \frac{a^2}{4}\left(\kappa - \frac{1}{\kappa}\right)^2 = 0, \quad \tilde{s} = hs. \quad (2.40)$$

Lemma

(i) (2.40) has no solutions with

$$|\kappa| = 1 \quad \text{for } \Re(\tilde{s}) > 0. \quad (2.41)$$

(ii) There are exactly two solutions κ_1, κ_2 with

$$|\kappa_j| < 1, \quad j = 1, 2 \quad \text{for } \Re(\tilde{s}) > 0. \quad (2.42)$$

(iii) For $\tilde{s} \rightarrow 0$,

$$\lim_{\tilde{s} \rightarrow 0} \kappa_1 = -\left(1 - \frac{2b}{a^2}\right) + \sqrt{\left(1 - \frac{2b}{a^2}\right)^2 - 1}, \quad \lim_{\tilde{s} \rightarrow 0} \kappa_2 = -\left(1 - \frac{2b}{a^2}\right) - \sqrt{\left(1 - \frac{2b}{a^2}\right)^2 - 1}. \quad (2.43)$$

Proof. Part (i) follows from the stability of the Cauchy problem, established in Sec. II A. For \tilde{s} real, as $\tilde{s} \rightarrow \infty$ the solutions of (2.40) with $|\kappa| < 1$ converge to the solutions of

$$\tilde{s}^2 + \frac{a^2}{4} \frac{1}{\kappa^2} = 0, \quad \text{i.e.} \quad \kappa_{1,2} = \pm \frac{ia}{2} \frac{1}{\tilde{s}}. \quad (2.44)$$

Correspondingly, the solutions of (2.40) with $|\kappa| > 1$ converge to the solutions of

$$\tilde{s}^2 + \frac{a^2}{4} \kappa^2 = 0, \quad \text{i.e.} \quad \kappa_{3,4} = \pm \frac{2\tilde{s}}{ia}. \quad (2.45)$$

Since the four roots $\kappa(\tilde{s})$ of (2.40) are continuous functions of \tilde{s} and $|\kappa| \neq 1$ for $\Re(\tilde{s}) > 0$, there are exactly two roots $\kappa_{1,2}$ with $|\kappa_{1,2}| < 1$ for all \tilde{s} with $\Re(\tilde{s}) > 0$, thus establishing (ii). For $\tilde{s} = 0$, we have

$$-b \frac{(\kappa - 1)^2}{\kappa} + \frac{a^2}{4} \frac{(\kappa^2 - 1)^2}{\kappa^2} = \frac{(\kappa - 1)^2}{\kappa} \left(-b + \frac{a^2}{4} \frac{(\kappa + 1)^2}{\kappa} \right) = 0, \quad (2.46)$$

i.e.

$$(\kappa - 1)^2 = 0 \quad \text{or} \quad (\kappa + 1)^2 - \frac{4b}{a^2} \kappa = \kappa^2 + 2\left(1 - \frac{2b}{a^2}\right)\kappa + 1 = 0. \quad (2.47)$$

Therefore,

$$\kappa_{1,2} = -\left(1 - \frac{2b}{a^2}\right) \pm \sqrt{\left(1 - \frac{2b}{a^2}\right)^2 - 1}, \quad \kappa_{3,4} = 1. \quad (2.48)$$

A simple perturbation analysis shows that $|\kappa_{3,4}| \sim |e^{\mu_{1,2}h}| > 1$ for $|\tilde{s}| \ll 1$, $\Re(\tilde{s}) > 0$, i.e. $\kappa_{3,4}$ correspond to the solution of (2.35). Since $a^2 > b$, we have $|\kappa_{1,2}| = 1$ for $\tilde{s} \rightarrow 0$ and (2.43) follows. This proves the lemma.

The lemma shows that $\sigma_3 = \sigma_4 = 0$. To account for possible double roots we write (2.39) as

$$u_\nu = e^{st} \left(\sigma_1 \kappa_1^\nu + \sigma_2 \frac{\kappa_2^\nu - \kappa_1^\nu}{\kappa_2 - \kappa_1} \right) \quad \text{if } \kappa_1 \neq \kappa_2, \quad (2.49)$$

which becomes

$$u_\nu = e^{st} (\sigma_1 \kappa_1^\nu + \sigma_2 \nu \kappa_2^{\nu-1}) \quad \text{if } \kappa_1 = \kappa_2. \quad (2.50)$$

Here σ_1, σ_2 are determined by the boundary conditions (2.38), i.e.

$$\begin{aligned} \sigma_1 (\kappa_1 - 1)^3 + \frac{\sigma_2}{\kappa_2 - \kappa_1} \left((\kappa_2 - 1)^3 - (\kappa_1 - 1)^3 \right) &= 0, \\ \sigma_1 \kappa_1 (\kappa_1 - 1)^3 + \frac{\sigma_2}{\kappa_2 - \kappa_1} \left(\kappa_2 (\kappa_2 - 1)^3 - \kappa_1 (\kappa_1 - 1)^3 \right) &= 0. \end{aligned} \quad (2.51)$$

The determinant of this system is

$$\text{Det} = (\kappa_1 - 1)^3(\kappa_2 - 1)^3. \quad (2.52)$$

We can now prove:

Theorem. (2.49), (2.51) has only the trivial solution ($\sigma_1 = \sigma_2 = 0$) for $\Re(s) \geq 0$. Therefore the difference approximation (2.37), (2.38) is stable.

Proof. By (2.52), we have $\kappa_1 = 1$ or $\kappa_2 = 1$. Then, by (2.40), $s = 0$ and, by (2.43), $\kappa_1 \neq 1$, $\kappa_2 \neq 1$, which is a contradiction. Therefore the Kreiss condition is satisfied. In Ch. 12 of [20], it is proved that the Kreiss condition implies stability.

Remark 1. The Ryabenkii-Godonov condition states that there are no bounded solutions of type (2.49) for $\Re(s) > 0$. The Kreiss condition requires that there are no bounded solutions for $\Re(s) \geq 0$. The Ryabenkii-Godonov condition is a necessary condition while the Kreiss condition is a sufficient condition for stability. (See Ch. 12 of [20].)

Remark 2. Mode analysis is closely connected with the Laplace transform. Therefore the stability estimates are expressed in terms of $\int_0^T \|u(\cdot, t)\|_h^2 dt$. As explained in Ch. 12 of [20], one can use these estimates to obtain standard energy estimates.

Remark 3. The stability theory in [19] and in Ch. 12 of [20] is only developed for first order systems. However, it generalizes directly to second order equations. Also in [19], it is indicated how to prove that the Principle of Frozen Coefficients holds. The approximation with smooth coefficients is stable if the system is strictly hyperbolic and the Kreiss condition holds.

D. Time discretization

The results in Sec's (IIB) and (IIC) prove that the outer algorithm gives a stable difference approximation for the halfplane problem with timelike boundary and that the horizon algorithm gives a stable difference approximation for the halfplane problem with a spacelike boundary. In Sec. (III), these results will be combined to give a stable difference approximation for the strip problem with spacelike inner boundary and timelike outer boundary.

For the time discretization, we use the method of lines. The spatial discretization reduces the problem to a large system of stable ODE's

$$\mathbf{u}_{tt} = \frac{1}{h} \mathbf{A} \mathbf{u}_t + \frac{1}{h^2} \mathbf{B} \mathbf{u}. \quad (2.53)$$

Introducing

$$\mathbf{u}_t = \frac{1}{h} \mathbf{v}, \quad (2.54)$$

we obtain the first order system

$$\begin{pmatrix} \mathbf{v} \\ \mathbf{u} \end{pmatrix}_t = \frac{1}{h} \begin{pmatrix} \mathbf{B} & \mathbf{A} \\ \mathbf{I} & \mathbf{0} \end{pmatrix} \begin{pmatrix} \mathbf{v} \\ \mathbf{u} \end{pmatrix}. \quad (2.55)$$

We solve the system numerically using a 4th order Runge-Kutta time integrator. The time step is limited by the CFL condition determined from the Cauchy problem.

III. THE LINEAR EXCISION PROBLEM

We model a pulse of energy propagating into a horizon using the wave equation

$$-\partial_t^2 u + \partial_t(a\partial_x u) + \partial_x(a\partial_t u) + \partial_x\left((1-a^2)\partial_x u\right) = 0 \quad (3.1)$$

on the interval $0 \leq x \leq 1$, where we set

$$\begin{aligned} a &= \frac{5}{4} - x, & 0 \leq x \leq \frac{1}{2} \\ a &= \alpha(x), & \frac{1}{2} \leq x \leq \frac{3}{4} \\ a &= \frac{1}{2}, & \frac{3}{4} \leq x \leq 1, \end{aligned} \tag{3.2}$$

with α providing a smooth monotonic transition between the inner and outer regions. The underlying metric is Lorentzian and (3.1) is hyperbolic. The inner boundary is spacelike, the outer boundary is timelike and there is an event horizon at $x = 1/4$.

The solution to (3.1) in the region $3/4 \leq x \leq 1$ has the exact form

$$u = f\left(t + \frac{2}{3}x\right) + g(t - 2x) \tag{3.3}$$

consisting of an ingoing wave f and an outgoing wave g . Near the inner boundary all waves are ingoing, as can be seen by freezing the coefficient a to obtain the solution

$$u = f\left(t + \frac{4}{9}x\right) + g(t + 4x), \tag{3.4}$$

which is valid in the short wavelength limit.

Our goal is to simulate a wave f incident on the boundary at $x = 1$ which propagates across the horizon, while being partially backscattered. We also check that a pulse of compact support inside the horizon does not propagate into the exterior region.

A. Linear algorithm with non-constant coefficients

First we must modify the evolution-boundary algorithm to account for non-constant coefficients, as required for the excision problem. We consider the equation

$$-\partial_t^2 u + \partial_t(a\partial_x u) + \partial_x(a\partial_t u) + \partial_x(c\partial_x u) = 0, \tag{3.5}$$

where $a = a(t, x)$ and $c = c(t, x)$. The energy associated with $t^\alpha \partial_\alpha = \partial_t$ is

$$E = \frac{1}{2} \int_0^1 (u_t^2 + cu_x^2) dx. \tag{3.6}$$

Note that for $c < 0$, E is not necessarily positive. For the case $a_t = c_t = 0$, energy conservation holds in the form

$$\partial_t E = F|_{x=1} - F|_{x=0} \tag{3.7}$$

where the boundary flux is

$$F = u_t(cu_x + au_t). \tag{3.8}$$

With this generalization, the homogeneous Dirichlet condition (2.16) remains $u_t = 0$ but the homogeneous Neumann condition (2.17) must be modified to

$$cu_x + au_t = 0. \tag{3.9}$$

We modify the outer algorithm to

$$W := u_{tt} - \partial_t(aD_0 u) - D_0(au_t) - \frac{1}{2}D_- \left((A_+c)D_+ u \right) - \frac{1}{2}D_+ \left((A_-c)D_- u \right) = 0, \tag{3.10}$$

where

$$A_\pm f_\nu = \frac{f_{\nu\pm 1} + f_\nu}{2}. \tag{3.11}$$

The last two terms in (3.10) are equal because of the identity

$$D_- \left((A_+ f) D_+ g \right) = D_+ \left((A_- f) D_- g \right), \quad (3.12)$$

but it is advantageous to express W in a form which is manifestly reflection invariant.

Consider now semi-discrete energy conservation for the case $a_t = c_t = 0$. We modify the semi-discrete version of the energy to

$$E = h \sum_1^{N-1} \mathcal{E} + \frac{h}{4} \left((u_{tN})^2 + (A_- c_N) (D_- u_N)^2 + (u_{t0})^2 + (A_+ c_0) (D_+ u_0)^2 \right) \quad (3.13)$$

where

$$\mathcal{E} = \frac{1}{2} u_t^2 + \frac{1}{4} (A_+ c) (D_+ u)^2 + \frac{1}{4} (A_- c) (D_- u)^2. \quad (3.14)$$

It follows that

$$\begin{aligned} \mathcal{E}_t - u_t W &= D_0 (a u_t^2) - \frac{h}{2} \left((D_+ u_t) D_+ (a u_t) - (D_- u_t) D_- (a u_t) \right) \\ &+ \frac{1}{2} u_t D_- \left((A_+ c) D_+ u \right) + \frac{1}{2} (D_+ u_t) (A_+ c) D_+ u \\ &+ \frac{1}{2} u_t D_+ \left((A_- c) D_- u \right) + \frac{1}{2} (D_- u_t) (A_- c) D_- u. \end{aligned} \quad (3.15)$$

Following the procedure leading to (2.25), the summation of this expression gives the semi-discrete flux conservation law

$$\begin{aligned} \partial_t E &= \frac{1}{2} u_{tN} \left(h W_N + (A_+ c_N) D_+ u_N + (A_- c_N) D_- u_N + (A_+ a_N) u_{t(N+1)} + (A_- a_N) u_{t(N-1)} \right) \\ &- \frac{1}{2} u_{t0} \left(-h W_0 + (A_+ c_0) D_+ u_0 + (A_- c_0) D_- u_0 + (A_+ a_0) u_{t1} + (A_- a_0) u_{t(-1)} \right). \end{aligned} \quad (3.16)$$

We express the Neumann condition (3.9) in the second order accurate form

$$\mathcal{N}' := \frac{1}{2} \left((A_+ c) D_+ u + (A_- c) D_- u + (A_+ a) T_+ u_t + (A_- a) T_- u_t \right) = 0, \quad (3.17)$$

where $T_{\pm} f_{\nu} = f_{\nu \pm 1}$. At the boundaries, \mathcal{N}'_N and \mathcal{N}'_0 contain ghost points outside the computational domain, which we eliminate via the relations

$$\frac{h}{2} W_N + \mathcal{N}'_N = \frac{h}{2} u_{ttN} + (A_- c_N) D_- u_N + (A_- a_N) u_{t(N-1)} \quad (3.18)$$

$$-\frac{h}{2} W_0 + \mathcal{N}'_0 = -\frac{h}{2} u_{tt0} + (A_+ c_0) D_+ u_0 + (A_+ a_0) u_{t1}. \quad (3.19)$$

Then, requiring that the wave equation be satisfied at the boundary points, i.e. that $W_N = W_0 = 0$, the conservation law (3.16) implies that the Neumann boundary conditions

$$\mathcal{N}'_N := \frac{h}{2} u_{ttN} + (A_- c_N) D_- u_N + (A_- a_N) u_{t(N-1)} = 0 \quad (3.20)$$

$$\mathcal{N}'_0 := -\frac{h}{2} u_{tt0} + (A_+ c_0) D_+ u_0 + (A_+ a_0) u_{t1} = 0 \quad (3.21)$$

are dissipative.

Energy conservation holds in the continuum theory only when the coefficients of the wave operator are time independent. However, in the continuum problem, conservation of the monopole quantity (2.30) holds for general

time-dependent coefficients in the case of homogeneous Neumann boundary conditions. This carries over to the conservation of the semi-discrete quantity

$$\mathcal{Q} = h \sum_{\nu=1}^{N-1} (u_{t\nu} - aD_0u_\nu) + \frac{h}{2}(u_{tN} - aD_-u_N + u_{t0} - aD_+u_0) \quad (3.22)$$

when the Neumann condition (3.17) has the correction

$$\mathcal{N} := \mathcal{N}' + \frac{h^2}{4}a_tD_+D_-u = 0, \quad (3.23)$$

which preserves second order accuracy. As a result of this correction, (3.20) and (3.21) are modified to

$$\frac{h}{2}W_N + \mathcal{N}_N := \frac{h}{2}(u_{ttN} - a_{tN}D_-u_N) + (A_-c_N)D_-u_N + (A_-a_N)u_{t(N-1)} = 0 \quad (3.24)$$

$$-\frac{h}{2}W_0 + \mathcal{N}_0 := -\frac{h}{2}(u_{tt0} - a_{t0}D_+u_0) + (A_+c_0)D_+u_0 + (A_+a_0)u_{t1} = 0. \quad (3.25)$$

Setting $W_\nu = 0$ for $1 \leq \nu \leq N-1$, a straightforward calculation then gives

$$\mathcal{Q}_t = \frac{h}{2}W_N + \mathcal{N}_N + \frac{h}{2}W_0 - \mathcal{N}_0. \quad (3.26)$$

Thus, again requiring that $W_N = W_0 = 0$, the boundary conditions

$$\mathcal{N}_N = \frac{h}{2}(u_{ttN} - a_{tN}D_-u_N) + (A_-c_N)D_-u_N + (A_-a_N)u_{t(N-1)} = 0 \quad (3.27)$$

$$\mathcal{N}_0 = -\frac{h}{2}(u_{tt0} - a_{t0}D_+u_0) + (A_+c_0)D_+u_0 + (A_+a_0)u_{t1} = 0, \quad (3.28)$$

imply $\mathcal{Q}_t = 0$. Thus we have established that $\mathcal{Q}_t = 0$ in the general case and $E_t = 0$ when the coefficients are frozen in time.

Note that when the coefficients are not frozen in time, an energy estimate still applies provided a, a_t, c, c_t are bounded functions, with $c > 0$. For simplicity, consider the case with periodic boundaries. Then for the continuum problem (3.5) and (3.6) imply

$$E_t = \int_0^1 (a_t u_t u_x + \frac{c_t}{2} u_x^2) dx. \quad (3.29)$$

The inequality $2fg \leq f^2 + g^2$ gives

$$a_t u_t u_x \leq \frac{|a_t|}{2\sqrt{c}} (u_t^2 + cu_x^2) \leq K_1 \mathcal{E} \quad (3.30)$$

where the constant K_1 satisfies $K_1 \geq |a_t|/\sqrt{c}$; and

$$\frac{c_t}{2} u_x^2 \leq \frac{|c_t|}{2c} (u_t^2 + cu_x^2) \leq K_2 \mathcal{E}, \quad (3.31)$$

where the constant K_2 satisfies $K_2 \geq |c_t|/c$. Integration of (3.29) then gives $E_t \leq (K_1 + K_2)E$ so that

$$E \leq E_0 e^{(K_1 + K_2)t}, \quad (3.32)$$

where E_0 is the initial energy. A straightforward calculation based upon the summation

$$E_t = h \sum_1^N (\mathcal{E}_t - u_t W) \quad (3.33)$$

leads to a semi-discrete energy estimate analogous to (3.32).

Finally, in the inner region, we modify the horizon algorithm (2.8) to the non-constant coefficient form

$$V := u_{tt} - \partial_t(aD_0u) - D_0(au_t) - \frac{1}{2}D_- \left((A_+b)D_+u \right) - \frac{1}{2}D_+ \left((A_-b)D_-u \right) + D_0(a^2D_0u) = 0, \quad (3.34)$$

where $c = b - a^2$.

B. Blending the outer and horizon algorithms

For the purpose of excision, we need a prescription for switching from the outer algorithm $W = 0$ to the horizon algorithm $V = 0$. We introduce a smooth, monotonic blending function $f(c) = f(b - a^2)$, satisfying $f = 1$ for $c \leq 0$ and $f = 0$ for $c \geq 1/2$. Referring to (3.10) and (3.34), we then use the blended evolution algorithm $B = 0$, where

$$B = W - D_- \left((A_+(fa^2))D_+u \right) + D_0 \left(fa^2D_0u \right) = W + \frac{h^2}{4} D_+ D_- (fa^2 D_+ D_- u), \quad (3.35)$$

which reduces to W near the outer boundary and to V inside the horizon.

When $\partial_t g^{\alpha\beta} = 0$, the blended algorithm satisfies a semi-discrete energy conservation law. For periodic boundary conditions (identifying the points $\nu = 0$ and $\nu = N$), this takes the form $\partial_t E_B = 0$ where

$$E_B = h \sum_1^N \mathcal{E}_B, \quad (3.36)$$

with

$$\mathcal{E}_B = \mathcal{E} + \frac{fh^2a^2}{8} (D_+ D_- u)^2. \quad (3.37)$$

(Here, as before, \mathcal{E} is not necessarily positive inside the horizon.)

For the boundary conditions of the excision problem, the energy (3.13) is modified in the same way,

$$E_B = E + h \sum_1^{N-1} \frac{fh^2a^2}{8} (D_+ D_- u)^2. \quad (3.38)$$

Since the support of the blending function f is isolated from the outer timelike boundary, the semi-discrete energy flux through the outer boundary remains given by the first term in (3.16).

C. Tests of the linear excision algorithm

In order to validate the linear algorithm a set of test-runs was performed where the outer boundary condition at $x = 1$ was either Dirichlet or Neumann, while at $x = 0$ the extrapolation conditions (2.38) were applied. The gridstep was chosen to be $h = 1/(\rho \cdot 2000)$, $\rho = 1, 2, 4$ with the time-step set to $\Delta t = h/10$. The background coefficients were set according to (3.2) with $\alpha(x) = 245/4 - 513x + 1728x^2 - 2880x^3 + 2368x^4 - 768x^5$ so that C^2 differentiability results.

In the first set of runs the initial data at $t = 0$ were a C^3 pulse of compact support inside the horizon with $u_t(0, x) = 0$ and

$$\begin{aligned} u(0, x) &= 0.5 \times [4\xi(1-\xi)]^4 \quad \text{for } x_0 \leq x \leq x_0 + 0.2 \\ u(0, x) &= 0 \quad \text{elsewhere,} \end{aligned} \quad (3.39)$$

with $\xi(\lambda) = (\lambda - 0.025)/0.2$. Homogeneous Dirichlet data $u(t, 1) = 0$ was given at the outer boundary. At the initial location of the pulse inside the horizon, both characteristics point to the left. The condition $u_t(0, x) = 0$ implies that the initial data is the superposition of two pulses, whose amplitudes have opposite signs, which propagate along these two characteristics. This is clearly seen in Fig. 1 where at first the “faster” mode (with small negative amplitude) falls into the excised region, while the “slower” mode (with positive amplitude) propagates in the same direction. We also monitor the convergence factor for the error modes that have propagated outside the horizon, defined in terms of the L_2 norm over the interval $x_H = 0.25 \leq x \leq 1$ as

$$\mathcal{C}(x \geq x_H) = \log_2 \left(\frac{\|u_{\rho=1}\|_2}{\|u_{\rho=2}\|_2} \right). \quad (3.40)$$

Second order accuracy would imply $\mathcal{C}(x \geq x_H) \geq 2$ since the analytic solution vanishes outside the horizon.

In the region outside the horizon, the simulation consists purely of short wavelength error. At first there is a high convergence rate but after about 6 crossing times the short wavelength error is unresolved on the grid. The addition

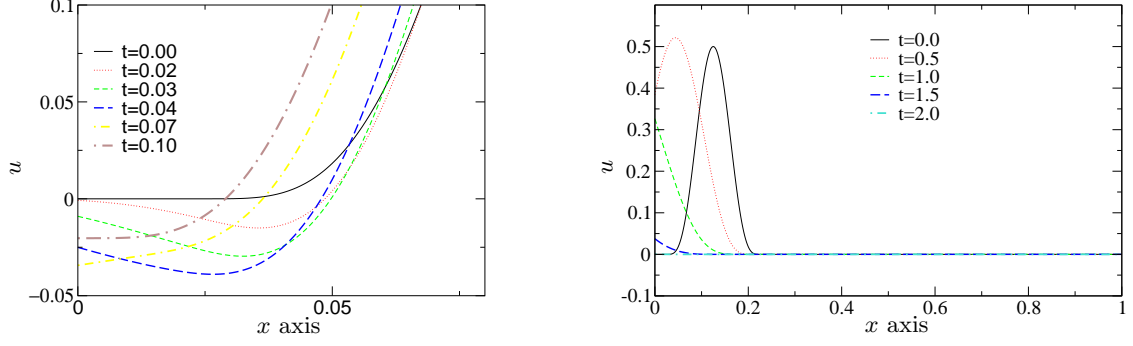


FIG. 1: Sequence of snapshots showing the initial pulse falling into the excised region. The left graph shows the early behavior as the faster mode (with negative amplitude) propagates through the excision boundary. The right graph shows the slower mode making its way through the excision boundary, with no observable trace remaining at $t = 2.0$.

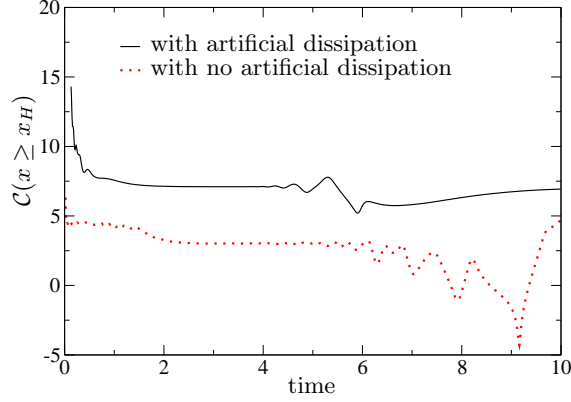


FIG. 2: Plot of the convergence factor $\mathcal{C}(x \geq x_H)$ as a function of time for the test run with an initial pulse inside the horizon. It is evident that the addition of dissipation is necessary for long term convergence.

of dissipation to the evolution scheme greatly extends the time for which convergence holds in the outer region, as shown in Fig. 2. Dissipation is added by modifying (2.55) according to

$$v_t \rightarrow v_t + \epsilon_v D_+ D_- F D_+ D_- v \quad (3.41)$$

$$u_t \rightarrow u_t + \epsilon_u D_+ D_- F D_+ D_- u, \quad (3.42)$$

where we set $\epsilon_v = \epsilon_u = 0.1 \cdot h^3$ and F is a smooth function with $F = b$ in the interior and $F = 0$ near both boundaries.

In the second set of runs, the initial Cauchy data were set to zero, $u(0, x) = u_t(0, x) = 0$, and a wave was introduced through the outer boundary $x = 1$ by prescribing inhomogeneous Neumann data

$$g^{x\alpha} \partial_\alpha u|_{x=1} = \left(\frac{3}{4} u_x + \frac{1}{4} u_t\right)|_{x=1} = q(t). \quad (3.43)$$

Figure 3 shows snapshots of the evolution for a wave generated by boundary data $q(t)$ consisting of a single pulse. The pulse enters the outer boundary in the incoming mode of (3.3) with characteristic velocity $-3/2$, propagates across the blending region and leaves the grid at the excision boundary. The figure also shows the remnant signal when no dissipation is added to the code. After the initial pulse has entered the outer boundary, the Neumann data is homogeneous and reflects any signal propagating to the right but signals propagating to the left can leave the system

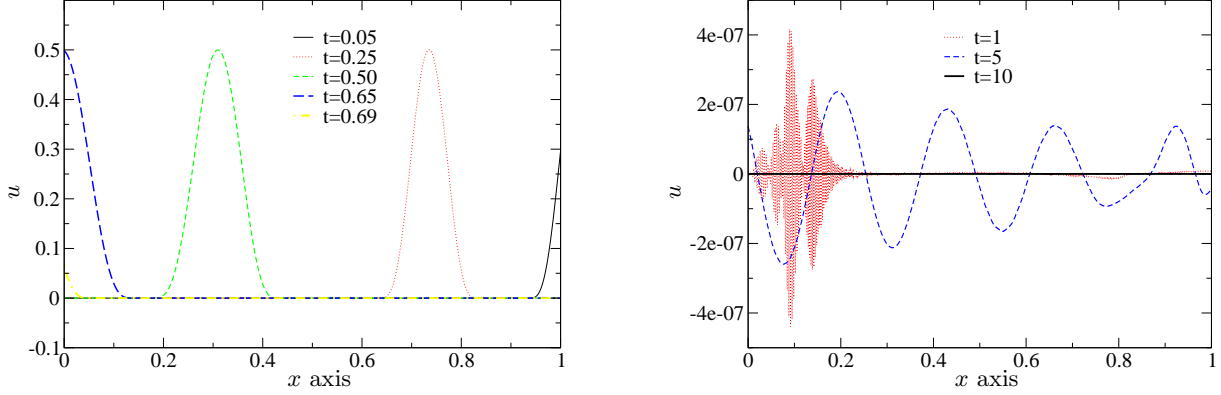


FIG. 3: Sequence of snapshots showing a pulse propagating across the grid. The left graph shows the propagation of the main signal, while the right graph illustrates the behavior of the residual error. The short wavelength error can be eliminated by dissipation.

across the excision boundary. At $t = 1$, short wavelength noise fills the region inside the horizon. By $t = 5$, the short wavelength error has either propagated through the excision boundary or has been converted into longer wavelengths. At $t = 10$, no visible signal remains. The short wavelength noise at $t = 1$ can be effectively eliminated by a small amount of dissipation.

We checked long term global convergence by prescribing a periodic wave entering through the outer boundary with the inhomogeneous Neumann data

$$\begin{aligned} q(t) &= 0, \quad \text{for } t < 1/150 \\ q(t) &= \left(c\partial_x + a\partial_t \right) \left[A \sin^4 \left(\pi [x - 1.01 + 1.5t] \right) \right] \Big|_{x=1}, \quad \text{for } t \geq 1/150. \end{aligned} \quad (3.44)$$

Again the initial Cauchy data was set to zero. The C^3 boundary data (3.44) is initially set to zero to provide C^∞ consistency with the Cauchy data. No artificial dissipation was added in this test.

We measured Cauchy convergence of the numerical solution by monitoring the convergence factor

$$C = \log_2 \left(\frac{\|u_{\rho=1} - u_{\rho=2}\|_2}{\|u_{\rho=2} - u_{\rho=4}\|_2} \right). \quad (3.45)$$

For the given data and grid sizes, the code displays second order accuracy to within less than one percent. Figure 4 plots the convergence factor as well as a snapshot of the residual finite difference error at the end of the simulation, at $t = 100$.

IV. THE QUASI-LINEAR EXCISION PROBLEM

A. Algorithms for the quasi-linear wave equation

We extend our algorithms to the quasi-linear wave equation (1.8) in such a way that the outer algorithm continues to obey a semi-discrete monopole conservation law in the case of homogeneous Neumann boundary conditions. We again set $c = b - a^2$ and treat the case of time-dependent, non-constant coefficients. We generalize the outer algorithm (3.10) to the finite-difference form

$$W := \partial_t \left(\frac{1}{\Phi} \Phi_t \right) - \partial_t \left(\frac{a}{\Phi} D_0 \Phi \right) - D_0 \left(\frac{a}{\Phi} \Phi_t \right) - \frac{1}{2} D_- \left(\left(A_+ \frac{c}{\Phi} \right) D_+ \Phi \right) - \frac{1}{2} D_+ \left(\left(A_- \frac{c}{\Phi} \right) D_- \Phi \right) = 0, \quad (4.1)$$

and generalize the horizon algorithm (3.34) to

$$V := \partial_t \left(\frac{1}{\Phi} \Phi_t \right) - \partial_t \left(\frac{a}{\Phi} D_0 \Phi \right) - D_0 \left(\frac{a}{\Phi} \Phi_t \right) - \frac{1}{2} D_- \left(\left(A_+ \frac{b}{\Phi} \right) D_+ \Phi \right) - \frac{1}{2} D_+ \left(\left(A_- \frac{b}{\Phi} \right) D_- \Phi \right) + D_0 \left(\frac{a^2}{\Phi} D_0 \Phi \right) = 0. \quad (4.2)$$

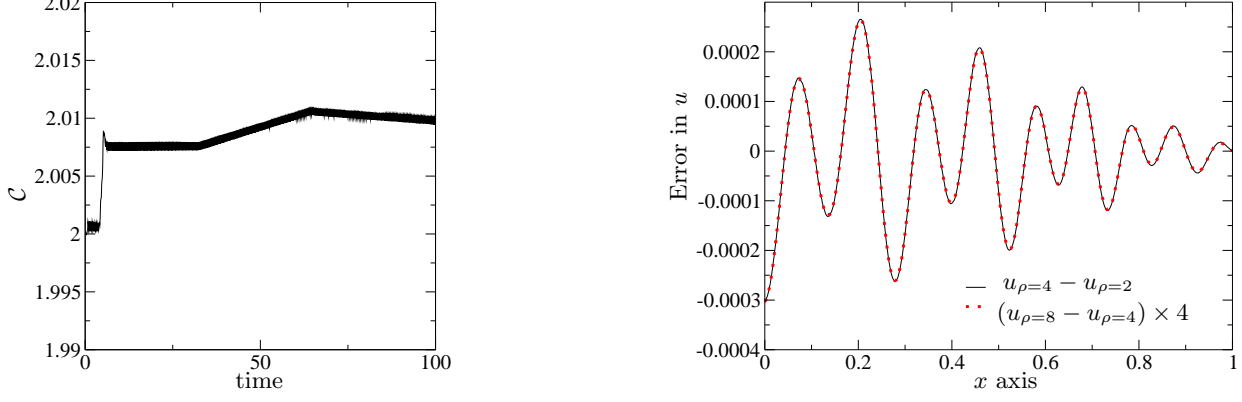


FIG. 4: Convergence plots for the test run with a periodic wave introduced through the outer (timelike) boundary. On the left, the plot of the convergence factor \mathcal{C} vs. time indicates good second order convergence up to the end of the simulation at $t = 100$. The quality of the long term performance is reinforced by the right graph which shows that, at the end of the simulation, the rescaled error profiles are in nearly perfect agreement. No artificial dissipation was introduced.

We blend these algorithms using the quasi-linear version of (3.35), i.e $B = 0$ with

$$B = W - D_- \left(\left(A_+ \frac{fa^2}{\Phi} \right) D_+ \Phi \right) + D_0 \left(\frac{fa^2}{\Phi} D_0 \Phi \right) = W + \frac{h^2}{4} D_+ D_- \left(\frac{fa^2}{\Phi} D_+ D_- \Phi \right). \quad (4.3)$$

As the boundary condition for the horizon algorithm at the spacelike excision boundary, we use the extrapolation conditions (2.38), now written as

$$h^3 D_+^3 \Phi_0 = 0, \quad h^3 D_+^3 \Phi_1 = 0. \quad (4.4)$$

Similarly, as homogeneous Dirichlet condition for the outer algorithm at a timelike outer boundary we retain the linear form $\Phi_t = 0$. We formulate the homogeneous Neumann condition for the outer algorithm to establish semi-discrete monopole conservation corresponding to the continuum conservation law

$$\partial_t \int_0^1 \left(\frac{\Phi_t}{\Phi} - \frac{a\Phi_x}{\Phi} \right) dx = 0. \quad (4.5)$$

We proceed as follows.

For periodic boundary conditions, (4.1) implies the semi-discrete conservation law $\partial_t \mathcal{Q} = 0$ where

$$\mathcal{Q} = h \sum_{\nu} \left(\frac{\Phi_{t\nu}}{\Phi_{\nu}} - \frac{a_{\nu} D_0 \Phi_{\nu}}{\Phi_{\nu}} \right). \quad (4.6)$$

This conservation law can be extended to a homogeneous Neumann boundary condition by adding boundary terms to (4.6) in the form

$$\begin{aligned} \mathcal{Q} &= h \sum_{\nu=1}^{N-1} \left(\frac{\Phi_{t\nu}}{\Phi_{\nu}} - \frac{a_{\nu} D_0 \Phi_{\nu}}{\Phi_{\nu}} \right) \\ &+ \frac{h}{2} \left(\frac{\Phi_{t0}}{\Phi_0} - \frac{a_0 D_+ \Phi_0}{\Phi_0} + \frac{\Phi_{tN}}{\Phi_N} - \frac{a_N D_- \Phi_N}{\Phi_N} \right). \end{aligned} \quad (4.7)$$

We generalize the Neumann condition (3.23) to the non-linear form

$$\mathcal{N} := \frac{1}{2} \left(\left(A_+ \frac{c}{\Phi} \right) D_+ \Phi + \left(A_- \frac{c}{\Phi} \right) D_- \Phi + \left(A_+ \frac{a}{\Phi} \right) T_+ \Phi_t + \left(A_- \frac{a}{\Phi} \right) T_- \Phi_t \right) + \frac{h^2}{4} \partial_t \left(\frac{a}{\Phi} \right) D_+ D_- \Phi = 0. \quad (4.8)$$

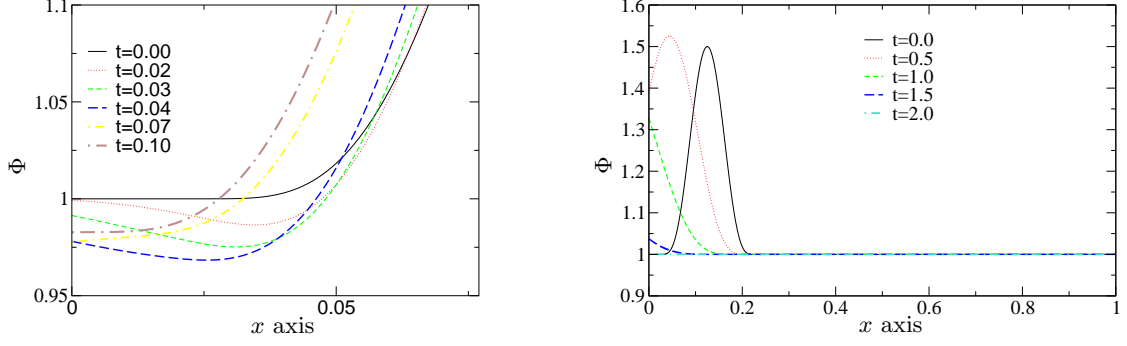


FIG. 5: Sequence of snapshots showing the initial pulse falling into the excised region, evolved with the quasi-linear system. The left graph shows the faster mode (with negative amplitude), while the right graph shows the slower mode making its way through the excision boundary. Grid-resolution for this simulation was $h = 1/8000$.

As a result of the nonlinearities, (3.24) and (3.25) are modified to

$$\frac{h}{2}W_N + \mathcal{N}_N := \frac{h}{2} \left(\partial_t \left(\frac{\Phi_{tN}}{\Phi_N} \right) - \partial_t \left(\frac{a_N}{\Phi_N} \right) D_- \Phi_N \right) + \left(A_- \frac{c_N}{\Phi_N} \right) D_- \Phi_N + \left(A_- \frac{a_N}{\Phi_N} \right) \Phi_{t(N-1)} \quad (4.9)$$

$$-\frac{h}{2}W_0 + \mathcal{N}_0 := -\frac{h}{2} \left(\partial_t \left(\frac{\Phi_{t0}}{\Phi_0} \right) - \partial_t \left(\frac{a_0}{\Phi_0} \right) D_+ \Phi_0 \right) + \left(A_+ \frac{c_0}{\Phi_0} \right) D_+ \Phi_0 + \left(A_+ \frac{a_0}{\Phi_0} \right) \Phi_{t1}. \quad (4.10)$$

Setting $W_\nu = 0$ for $1 \leq \nu \leq N-1$, a straightforward calculation leads to the nonlinear version of (3.26), i.e.

$$\mathcal{Q}_t = \frac{h}{2}W_N + \mathcal{N}_N + \frac{h}{2}W_0 - \mathcal{N}_0. \quad (4.11)$$

We implement the homogeneous Neumann condition in the form

$$\mathcal{N}_N = \frac{h}{2} \left(\partial_t \left(\frac{\Phi_{tN}}{\Phi_N} \right) - \partial_t \left(\frac{a_N}{\Phi_N} \right) D_- \Phi_N \right) + \left(A_- \frac{c_N}{\Phi_N} \right) D_- \Phi_N + \left(A_- \frac{a_N}{\Phi_N} \right) \Phi_{t(N-1)} = 0 \quad (4.12)$$

$$\mathcal{N}_0 = -\frac{h}{2} \left(\partial_t \left(\frac{\Phi_{t0}}{\Phi_0} \right) - \partial_t \left(\frac{a_0}{\Phi_0} \right) D_+ \Phi_0 \right) + \left(A_+ \frac{c_0}{\Phi_0} \right) D_+ \Phi_0 + \left(A_+ \frac{a_0}{\Phi_0} \right) \Phi_{t1} = 0. \quad (4.13)$$

Then the requirement that $W_N = W_0 = 0$ leads to the semi-discrete monopole conservation $\mathcal{Q}_t = 0$.

B. Tests of the quasi-linear excision algorithm

The excision tests performed with the quasi-linear code were based upon the ones performed with the linear code, with the (time independent) coefficients of the wave operator having spatial dependence determined by (3.2) and with the same Cauchy data or boundary data now prescribed for $(\Phi - 1)$ as were prescribed for the linearized field u in Sec. III C.

The initial data for the first set of runs consisted of a pulse of compact support inside the horizon with homogeneous Dirichlet data at the outer boundary. The initial peak amplitude of the pulse (3.39) was $\Phi_{max} = 1.5$, putting it in the nonlinear regime. Since the characteristic speeds determined by the background metric are the same as in the linearized case, the snapshots of the quasi-linear evolution shown in Fig. 5 are qualitatively similar to the linearized ones in Fig. 1. There is no visible propagation of the signal into the region outside the horizon. The convergence factor $\mathcal{C}(x \geq x_H)$ for the error modes that have propagated outside the horizon is defined by replacing u by $(\Phi - 1)$ in (3.40). As in the linear case, the short wavelength error in the exterior region is unresolved on the grid. The plots in Fig. 6 show that dissipation must be added to the code to obtain long term convergence.

In the second set of non-linear runs, the initial Cauchy data were set to zero and a wave introduced through the outer boundary by prescribing inhomogeneous Neumann data. Figure 7 shows snapshots of the evolution for a wave

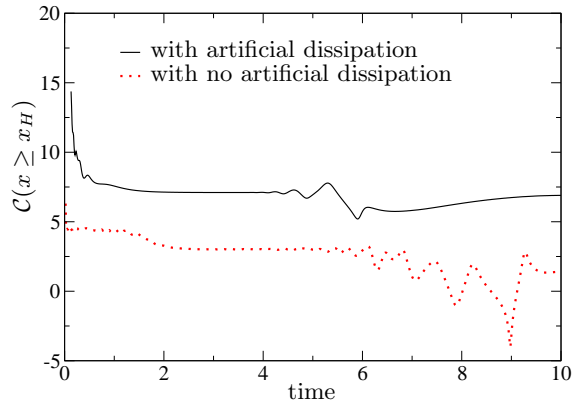


FIG. 6: Plot of the convergence factor $\mathcal{C}(x \geq x_H)$ vs. time. for the non-linear test run for an initial pulse inside the horizon. Addition of dissipation is necessary for long term convergence.

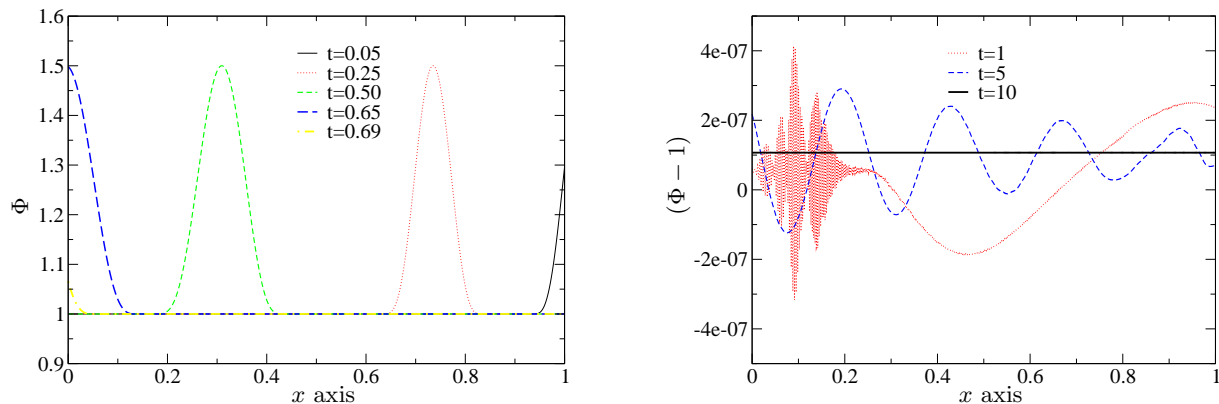


FIG. 7: Sequence of snapshots showing a pulse propagating across the grid with resolution $h = 1/2000$. The left graph shows the propagation of the signal itself, while the right graph illustrates the behavior of the residual modes. The long wavelength mode, which is apparent at $t = 1$, decays by $t = 5$ and no visible signal remains at $t = 10$.

consisting of a single pulse entering the outer boundary. No artificial dissipation was used. The main signal behaves qualitatively similar to the linearized case in Figure 3 but the error modes behave differently. At $t = 1$ the short wavelength error again fills the region inside the horizon but now long wavelength error has also been excited which extends to the outer boundary. This corresponds to mixing in the exponential modes

$$\Phi = e^{\lambda(t - \frac{2x}{3})}, \quad (4.14)$$

which are exact solutions (for any λ) to the quasi-linear wave equation (1.8) in the region $x \geq 3/4$. These modes are consistent with the homogeneous Neumann boundary condition (3.43) in effect after the pulse has entered the system and $q(t)$ vanishes. However, the mode (4.14) is not excited with positive λ and decays by $t = 5$. No visible signal remains at $t = 10$. Thus the discrete monopole conservation built into the quasi-linear system suppress exponentially growing long wavelength modes.

A further test of long term performance is the introduction of a periodic wave through the outer boundary by prescribing the inhomogeneous Neumann data (3.44). We measured Cauchy convergence by monitoring the convergence factor \mathcal{C} (3.45) applied to the numerical solution for Φ . Figure 8 plots \mathcal{C} as well as a snapshot of the residual finite difference error at $t = 100$, when the simulation was ended. The code displays second order accuracy to better than 1 percent. No artificial dissipation was used in the test.

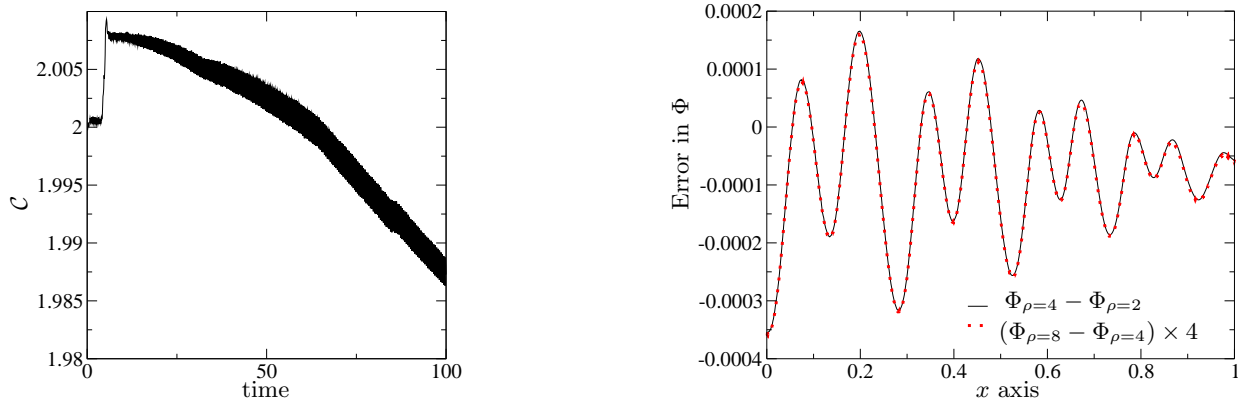


FIG. 8: Convergence plots for the non-linear test run with a periodic pulse introduced through the outer (timelike) boundary. On the left, the time dependence of the convergence factor \mathcal{C} indicates good second order convergence. This result is reinforced by the right graph where, at the end of the simulation at $t = 100$, the rescaled error profiles show a nearly perfect agreement. No artificial dissipation was used in this test.

V. DISCUSSION

We have based successful simulations of the model excision problem for a 1-dimensional quasi-linear wave equation on evolution and boundary algorithms which were proved to be stable in the linear case. The quasi-linear algorithm incorporates a conserved scalar monopole moment which suppresses the excitation of long wavelength exponentially growing modes, such as (4.14), which are latent in the system when Neumann boundary conditions are used. The global excision strategy involves matching an exterior evolution algorithm to a horizon algorithm for evolution of the interior region. The exterior algorithm admits simple implementation of an outer boundary condition and it obeys a discrete version of flux-energy conservation which guarantees stability. Inside the horizon, this energy is not positive-definite and the exterior algorithm is unstable. The horizon algorithm is stable in the interior region and admits a stable extrapolation algorithm to update the spacelike excision boundary. The choice of horizon algorithm presented here is based upon centered differencing. Other choices are possible in the model 1-dimensional problem. In particular, a horizon algorithm based completely upon one-sided differencing is stable and requires no extrapolation at the inner boundary. This would be a very attractive feature if it could be extended to the higher dimensional problem.

Preliminary investigations indicate that the computational algorithms presented here can be taken over in a fairly straightforward manner to the harmonic formulation of the full 3-dimensional gravitational problem. In that case the Einstein equations reduce to to the quasi-linear form

$$\frac{1}{\sqrt{-g}} \partial_\alpha (\sqrt{-g} g^{\alpha\beta} \partial_\beta g^{\mu\nu}) = S^{\mu\nu}, \quad (5.1)$$

where $S^{\mu\nu}$ consists of lower differential order terms which do not contribute to the principle part. These equations have a well-posed initial-boundary value problem when the boundary data is explicitly prescribed [2].

The principle part of (5.1) can be treated in the same way as a quasi-linear wave equation (1.2) for each component of the metric. From the point of view of designing a code, the two main differences from our model excision problem are (i) the the 3-dimensional nature of the full problem and (ii) the constraints which enter into the boundary conditions.

The evolution algorithms readily extend to 3-dimensions. When $S^{\mu\nu}$ is neglected, the flux conservative form of (5.1) can be carried over to the 3 dimensional discretized system to obtain discrete analogues of the scalar wave monopole conservation. There results a conserved quantity representing a spatially averaged rate of growth for each metric component, which has monopole symmetry for the g^{tt} component, dipole symmetry for the g^{ti} components and quadrupole symmetry for the g^{ij} components. The exact form of the conserved quantities depends upon how the principle part is split off in conservative form, with (5.1) just one possibility. See the discussion in [9] for how a splitting analogous to the logarithmic form (1.8) for the quasi-linear scalar problem leads to accurate long term simulation of the gauge wave problem; it remains to be seen if this splitting is effective in more general spacetimes. When $S^{\mu\nu}$ is neglected and the metric coefficients in the wave operator are frozen, semi-discrete energy conservation

also results for each metric component in the case of periodic boundary conditions. With a cubic grid boundary, the results for the quasi-linear wave equation generalize to dissipative Dirichlet and Neumann boundary conditions for the metric components. The chief complication is the application of Neumann conditions at the edges and corners of the cube. Here among possible approaches are the use of the *summation by parts* technique, as in [12], or the introduction of a smooth boundary which is treated by interpolation, as in [16, 17].

The constraints on the boundary data present another complication. The constraints on the system (5.1), which guarantee that the solutions satisfy Einstein's equations, are the harmonic coordinate conditions

$$\partial_\nu(\sqrt{-g}g^{\mu\nu}) = \hat{H}^\mu \quad (5.2)$$

where \hat{H}^μ are explicit harmonic driving functions. These constraints are satisfied by the solutions of (5.1) if a certain mixture of Dirichlet and Neumann boundary conditions are used for the metric components [2]. In that case, the constraints are satisfied when homogeneous boundary data are given and the initial-boundary problem for Einstein's equations is well-posed. In the case of inhomogeneous constraint-preserving boundary data it is not known whether the system remains well-posed.

It should be emphasized that, in addition to the computational difficulty, there are analytic and geometric problems in treating black holes. There is the possibility of exponentially growing perturbations to the analytic problem in the inner region near the excision boundary. There is the nonlocal nature of the *true* (null) event horizon. Although the spacelike apparent horizon can be traced out as the evolution proceeds, it is impossible to locate the null event horizon until the exterior evolution is complete. The matching of an inner horizon algorithm to an outer algorithm must be carried out across an artificial horizon which results from a given choice of shift, as in our model problem. In the black hole excision problem, such an artificial horizon could be defined in terms of the hypersurface across which the evolution goes from superluminal to subluminal.

Pretorius [3] has recently obtained promising results using a second order harmonic code to simulate a black hole by means of excision. We are now in the process of applying the new techniques presented here to this problem.

Acknowledgments

We thank M. Babiuc, L. Lehner and M. Tiglio for their input. This work was supported by the National Science Foundation under grant PH-0244673 to the University of Pittsburgh.

-
- [1] D. Garfinkle, *Phys.Rev.*, **D65**, 044029 (2002).
 - [2] B. Szilágyi and J. Winicour, *Phys. Rev.*, **D68**, 041501 (2003).
 - [3] F. Pretorius, *Class.Quant.Grav.* **22**, 425 (2005).
 - [4] R. Arnowitt, S. Deser and C. Misner, in *Gravitation: An Introduction to Current Research*, ed. L. Witten (New York, Wiley, 1962).
 - [5] G. Calabrese, L. Lehner, D. Neilsen, J. Pullin, O. Reula, O. Sarbach, and M. Tiglio, *Class. Quant. Grav.* **20**, L245, (2003).
 - [6] G. Calabrese, *Phys.Rev. D* **71**, 027501 (2005).
 - [7] www.appleswithapples.org
 - [8] M. Alcubierre, *et al*, *Class. Quantum Grav.*, **21**, 589 (2004).
 - [9] "Some mathematical problems in numerical relativity", M. Babiuc, B. Szilágyi and J. Winicour, gr-qc/0404092.
 - [10] M. Tiglio, L. Lehner, D. Neilsen, *Phys.Rev. D* **70**, 104018 (2004).
 - [11] H.-O. Kreiss and G. Scherer, *SIAM J. Numer. Anal.* **29**, 640 (1992).
 - [12] G. Calabrese, L. Lehner, O. Reula, O. Sarbach, and M. Tiglio, *Class.Quant.Grav.* **21**, 5735 (2004).
 - [13] L. Lehner, D. Neilsen, O. Reula and M. Tiglio, *Class.Quant.Grav.* **21**, 5819 (2004).
 - [14] H.-O. Kreiss, N. A. Peterson and J. Yström, *SIAM J. Numer. Anal.* **40**, 1940 (2002).
 - [15] H.-O. Kreiss and O. E. Ortiz, *Lect. Notes Phys.*, **604**, 359 (2002).
 - [16] "A second order accurate embedded boundary method for the wave equation with Dirichlet data", H.-O. Kreiss and N. A. Peterson, preprint UCRL-JRNL-202686, Lawrence Livermore National Lab (2004).
 - [17] "Difference approximations of the Neumann problem for the second order wave equation", H.-O. Kreiss, N. A. Peterson and J. Yström, preprint UCRL-JC-153184, Lawrence Livermore National Lab (2003).
 - [18] M. Alcubierre and B. Schutz, *J. Comput. Phys.*, **112**, 44 (1994).
 - [19] B. Gustafsson, H.-O. Kreiss and A. Sundstrom, *Mathematics of Computation*, **26**, 649 (1972).
 - [20] B. Gustafsson, H.-O. Kreiss and J. Olinger, *Time Dependent Problems and Difference Methods* (Wiley, NY, 1995).